Rigorous computational study reveals what docking overlooks : Double trouble from membrane association in protein kinase C modulators

Lautala, Saara

American Chemical Society
2020-11-23

Lautala, S, Provenzani, R, Koivuniemi, A, Kulig, W, Talman, V, Rog, T, Tuominen, R K, Yli-Kauhaluoma, J & Bunker, A E 2020, 'Rigorous computational study reveals what docking overlooks : Double trouble from membrane association in protein kinase C modulators', Journal of Chemical Information and Modeling, vol. 60, no. 11, pp. 5624-5633. https://doi.org/10.1021/acs.jcim.0c006

http://hdl.handle.net/10138/334259
10.1021/acs.jcim.0c00624

unspecified
acceptedVersion

Rigorous computational study reveals what docking overlooks: Double trouble from membrane association in protein kinase C modulators

Saara Lautala,[†] Riccardo Provenzani,[‡] Artturi Koivuniemi,[†] Waldemar Kulig,[¶] Virpi Talman,[§,‖] Tomasz Róg,[¶] Raimo K. Tuominen,[§] Jari Yli-Kauhaluoma,[‡] and Alex Bunker*[,†]

†*Drug Research Program, Division of Pharmaceutical Biosciences, P.O. Box 56 (Viikinkaari 5 E), FI-00014 University of Helsinki, Finland*

‡*Drug Research Program, Division of Pharmaceutical Chemistry and Technology, P.O. Box 56 (Viikinkaari 5 E), FI-00014 University of Helsinki, Finland*

¶*Department of Physics, University of Helsinki, P.O. Box 64 (Gustaf Hällströmin katu 2), FI-00014 University of Helsinki, Finland*

§*Drug Research Program, Division of Pharmacology and Pharmacotherapy, P.O. Box 56 (Viikinkaari 5 E), FI-00014 University of Helsinki, Finland*

‖*National Heart and Lung Institute, Imperial College London, Hammersmith campus, London, W12 0NN, United Kingdom*

E-mail: alex.bunker@helsinki.fi

Abstract

Increasing protein kinase C (PKC) activity is of potential therapeutic value. Its activation involves an interaction between the C1 domain and diacylglycerol (DAG) at intracellular membrane surfaces; DAG mimetics hold promise as new drugs. We previously developed the isophthalate derivative HMI-1a3, an effective but highly lipophilic (clog$P$ = 6.46) DAG mimetic. Although a less lipophilic pyrimidine analog, PYR-1gP (clog$P$ = 3.30), gave positive results in computational docking, it unexpectedly presented greatly diminished binding to PKC *in vitro*. Through more rigorous computational molecular modeling, we reveal that, unlike HMI-1a3, PYR-1gP forms an intramolecular hydrogen bond, which both obstructs binding and reorients PYR-1gP in the membrane in a fashion that prevents it from correctly accessing the PKC C1 domain. Our results highlight the great value of molecular dynamics simulations as a key component for the drug design process of ligands targeting weakly membrane-associated proteins, where simulation in the relevant membrane environment is crucial for obtaining biologically applicable results.

Introduction

The enzyme protein kinase C (PKC) plays a plethora of roles in human physiology, thus also many diseases, including cancer, diabetes, heart failure and Alzheimer's disease.[1–3] While previously thought to be an oncoprotein, recent studies of PKC, however, indicate that mutations associated with increased risk of cancer development result in a decrease, rather than increase, in PKC activity.[1] Prolonged activation by strong agonists, however, leads to the downregulation of PKC, which may be responsible for the tumor-promoting activity of ultrapotent PKC activators, for example phorbol esters.[1] Moderate activation of PKC with weaker agonists or partial agonists that do not cause the downregulation of PKC has therefore been proposed as tumor suppressing.[1,4] In addition, PKC is involved in learning and memory formation; moderate activation has also been proposed as a possible treatment

for Alzheimer's disease.[2,3]

Several isoenzymes of PKC exist and can be divided into three families based on their mode of activation: classical, novel and atypical. All PKC isoenzymes are peripheral membrane proteins; in their dormant state they reside in the cytoplasm, however activation and function occur at the surface of an intracellular membrane, *e.g.* the cytoplasmic leaflet of the plasma membrane.[1,2] For two out of the three families, the classical and novel, a physiological activator is the lipid second messenger diacylglycerol (DAG), which binds to PKC in a transient fashion and contributes to the activation of the enzyme.[1,2] In both classical and novel isoenzymes, the domains that possess affinity for DAG are the two tandem cysteine-rich domains, C1A and C1B.[1,2] Thus, regarding the structural design for DAG mimetics, the interaction between these domains and prospective agonists is of interest.[5,6]

This interaction is mainly governed by hydrogen bonds (H-bonds) between the glycerol backbone of DAG and the protein, most importantly the hydroxy group (−OH) in the *sn*-3 position of the glycerol (red in Figure 1) and the ester group oxygens in the *sn*-1 and *sn*-2 positions (green in Figure 1) and the protein.[7–9] Previously, we developed hydrophobic isophthalic acid derivatives (HMIs) as DAG mimetics, in order to achieve the desired modulation in classical and novel isoenzymes of PKC.[8] The ligands in this scaffold possess a trisubstituted phenyl ring with two ester functions in positions 1 and 5, bearing hydrophobic substituents, and a hydroxymethyl moiety ($-CH_2OH$) in position 3. These features mimic the *sn*-1,2–bound fatty acids and the *sn*-3–bound −OH group of DAG, respectively; they are designed to maintain the binding moieties at a comparable distance at the lipid–water interface while retaining the amphipathic properties of DAG. One compound, HMI-1a3 (Figure 1), showed significant promise in *in vitro* competitive binding assays against the radiolabeled phorbol ester [^{3}H]PDBu and also on *in vitro* assays on prostate cancer and HeLa cervical carcinoma cells.[10,11] The compound's low solubility in water, due to its high lipophilicity (clog$P$ = 6.46), however, could prevent its use as a viable drug candidate.

In our previous work, we designed and synthesized a set of HMI analogs with reduced

lipophilicity using scaffold hopping, in order to increase their potential viability as drug candidates.[9] The new candidate ligands featured a more hydrophilic pyrimidine in place of the hydrophobic phenyl core of the HMIs, while maintaining the binding moieties and hydrophobic substituents. Among the resulting compounds, the more hydrophilic analog of HMI-1a3, PYR-1gP ($\mathrm{clog}P = 3.30$) (Figure 1) matched the performance of HMI-1a3 in the *in silico* ligand docking study. Surprisingly, the experimental competitive binding assay showed greatly diminished binding for this analog, as PYR-1gP failed to displace [^{3}H]PDBu from PKCα in the presence of phosphatidylserine membranes.[8,9]

Failure of the *in silico* docking study to correctly predict the result of the biological assay is not unexpected, as the technique used is known to be oversimplified.[12] One notable factor that is often dismissed is the effect of the exact environment in which the binding takes place. For the case of PKC agonists, the binding occurs at the water-membrane interface, which has a complex, inhomogeneous structure.[13] So far, ligand design has mostly overlooked the role played by the lipid membrane in the ligand–protein interaction, for the most part due to the previous studies predating the development of the needed methodology and computational power.

In this study, we used molecular modeling, in tandem with quantum mechanical electronic structure calculation (QM) and NMR spectroscopy experiment, to investigate the mechanism responsible for the failure of the pyrimidine analog PYR-1gP to bind to the C1 domain of PKC in spite of the fact that docking studies suggested favorable interactions for binding. Multifaceted molecular modeling methods were used, combining molecular dynamics (MD) simulations (classical and steered) with free energy calculations using thermodynamic integration (TI). We hypothesized that the lipid membrane plays a crucial role in ligand selection; failure to include its presence in the model is the cause of the lack of correlation between *in silico* docking calculation and *in vitro* binding assays. In our simulations, we considered HMI-1a3 and PYR-1gP in the explicit lipid membrane environment, both with and without the target protein present. Altogether, our goal was to obtain a comprehensive

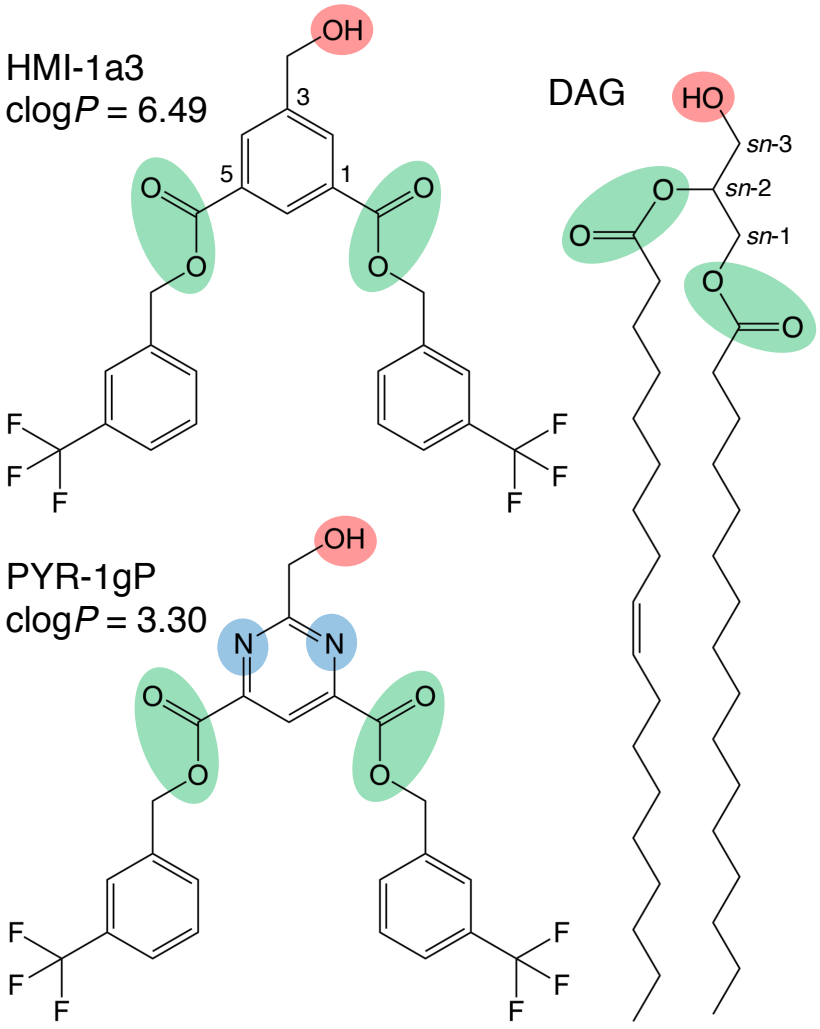

Figure 1: Structures of the two investigated compounds HMI-1a3 and PYR-1gP along with an example of the physiological PKC activator diacylglycerol (DAG; 1-palmitoyl-2-oleoyl-*sn*-glycerol *i.e.* POG). The functional groups, required for the binding to the C1 domain of PKC, are highlighted; the hydroxy (−OH) groups highlighted in red and the ester group oxygens in green. The nitrogen atoms, that differentiate the compounds, are highlighted in blue.

picture of the intrinsic behavior of the ligands inside the lipid bilayer, in order to shed light on how the membrane affects the ligand binding modes of PKC and possibly other weakly membrane-associated proteins. Through our study, we determined that the membrane does indeed play a role in binding affinity; the membrane environment pushes PYR-1gP to form an intramolecular H-bond between the −OH moiety and the pyrimidine ring, which significantly reduces affinity through two mechanisms: 1) the −OH is directly occupied by the internal H-bond and 2) the ligand is reoriented in an unfavorable fashion. Interestingly, the experimental NMR study, together with QM calculations, demonstrated that this bond is less prominent in a polar solvent; the apolar lipid membrane with which the ligand is associated was thus found to be the dominant factor regarding all causes of the difference in affinity between the two ligands.

Materials and methods

Computational methods

Electronic structure calculations

All quantum calculations (QM) were performed using Gaussian16 software.[14] Initial geometry optimization for both of the compounds was performed using density functional theory using the Becke B3LYP exchange correlation functional[15,16] with Pople's[17] polarized split valence double zeta basis set 6-31G*. Water solvent conditions were simulated in these calculations using the polarizable continuum model (PCM)[18–20] with the integral equation formalism variant (IEFPCM) as implemented in Gaussian16.[14] The resulting structures were further optimized, using the same functional, with a larger Dunning[21] correlation-consistent triple zeta basis set with added diffusion functions (aug-cc-pVTZ), with the same PCM conditions. The electrostatic potential around the molecules was computed using the Merz-Singh-Kollman scheme[22] using 10 layers and 13 gridpoints per unit area with identical condi-

tions to that used for the geometry optimization. The RESP fit procedure was then utilized as implemented in the AmberTools18 Antechamber to obtain the final partial charges for the compounds.[23–25] The conformational energies for certain dihedrals of HMI-1a3 and PYR-1gP, needed for both parametrization and analysis, were calculated by rotating the dihedral in question in 20° intervals between −180° and 180°, then performing a geometry optimization and finally a single point energy calculation for the optimized structure in each conformation at the same B3LYP/aug-cc-pVTZ[15,16,21] level as before. The calculation was repeated for both compounds in PCM conditions to simulate a water environment and in a vacuum to simulate the apolar lipid environment.[18–20] For efficiency, the dihedral parameters were derived using a sufficient fraction of the actual structure with all groups that could play a role in the energy present (see Figure S7). PCM calculations were utilized for the final parameterization for consistency with the partial charges. See the Supplementary Information (SI) for further details regarding how the potentials were fitted to the OPLS-AA force field and discussion of the parameterization.

Simulated systems

The membranes used in the simulations were assembled using the CHARMM-GUI membrane builder engine.[26,27] The crystal structure of the relevant domain of PKC, PKCδ-C1B (PDB:1PTR),[28] previously used for the docking studies,[8,9] was also used for the TI calculations. The reason this structure was used is that to date a high-resolution structure of PKCα C1 domain with a relevant ligand bound remains unsolved. The protein and ligand molecules were parametrized with the OPLS-AA parameter set,[29] and their topologies were built using the Gromacs *pdb2gmx* command and the MKtop script, respectively.[30–32] For the ligand molecules, partial charges and missing dihedrals were calculated at QM level as described in the previous section. The lipids were modeled using the previously published OPLS-AA compatible lipid-parameter set.[33,34] The membrane systems used in our simulations were chosen to model the *in vitro* test assay used in the aforementioned previous work.[8,9] The

only lipids used in the experiments were bovine brain-derived phosphatidylserines, thus all of our systems were composed of only 1-stearoyl-2-docosahexaenoyl-*sn*-glycero-3-phospho-L-serine (18:0-22:6(*n*-3) PS, SDPS). This composition does not reflect any endogenous lipid membrane; it was selected solely to ensure full compatibility between the simulation results and the experimental assay, as our goal was to explain the specific experimental results obtained previously. All models were solvated in TIP3P water model and K^+ counterions were added to preserve charge neutrality of the model.[35,36] Simulations were performed both with and without the protein C1B domain present. Further details related to system preparation and composition can be found in the SI.

Classical and steered molecular dynamics

Two separate classical unbiased MD simulations independent of the PKC protein, one for each of the ligands, HMI-1a3 and PYR-1gP, were carried out to investigate their behavior in the membrane. As a first step of building the systems for these simulations, we determined that, in all cases, the compounds we studied entered the membrane spontaneously when initialized in the solvent phase in 100–300 ns simulation time (see Figure S3). This justified the decision to perform further simulations, with the compounds initialized in the membrane core, for sampling efficiency. In both simulations, four laterally separated molecules of each of the compounds were initialized within the membrane core and simulated for 1.2 µs, in total, each. Equilibration was deemed to have occurred, effectively, by ∼100 ns in both systems, thus the latter 1.1 µs of the simulation trajectory was used for analysis. More details regarding the equilibration procedure can be found in the SI.

In the steered MD simulations, we manually removed the internal H-bond of PYR-1gP by reversing the potential on the specific dihedral interaction that controls its formation, *i.e.* adding a biasing potential (see Figure S8). The steered system was identical to the classical unbiased system in terms of other components and only the ligand molecules were affected by the added bias potential. The biased system (PYR-M1gP) was simulated for 600 ns with

the last 500 ns of the trajectory used for analysis.

Thermodynamic integration

As the docking in our previous studies had suggested similar binding to the relevant domain, PKCδ-C1B (PDB:1PTR),[28] for both of the compounds,[8,9] we also calculated the relative difference in the free energy of binding by thermodynamic integration.[37] In these simulations, we alchemically transformed HMI-1a3, docked into a membrane-embedded C1B domain, into PYR-1gP through a series of simulations, *i.e.* intermediate states, and subsequently calculated the relative free energy change along this path: $\Delta\Delta G^{\text{protein}}_{\text{HMI}-1a3\rightarrow\text{PYR}-1gP}$. The lipid environment, however, adds an additional energy contribution to the result so we also performed the same transformation and energy calculation in the lipid bilayer, independent of the protein (see Figure 2 for illustration). With this approach we obtained two results for the free energy difference of the transformation from HMI-1a3 to PYR-1gP with the lipid environment contributions added: $\Delta G^{\text{membrane}}_{\text{HMI}-1a3\rightarrow\text{PYR}-1gP}$ and $\Delta G^{\text{membrane+protein}}_{\text{HMI}-1a3\rightarrow\text{PYR}-1gP}$. We could thus obtain the final value for the change in relative free energy of binding without the lipid environment contributions by subtracting these two values:

$$\Delta\Delta G^{\text{protein}}_{\text{HMI}-1a3\rightarrow\text{PYR}-1gP} = \Delta G^{\text{protein+mebrane}}_{\text{HMI}-1a3\rightarrow\text{PYR}-1gP} - \Delta G^{\text{mebrane}}_{\text{HMI}-1a3\rightarrow\text{PYR}-1gP}.$$

Each simulation set was composed of 21 intermediate states; the $\Delta G^{\text{membrane}}_{\text{HMI}-1a3\rightarrow\text{PYR}-1gP}$ calculations were run for 60 ns per state, and the $\Delta G^{\text{membrane+protein}}_{\text{HMI}-1a3\rightarrow\text{PYR}-1gP}$ calculations were run for 13 ns per state. The convergence of the TI was observed to be almost instantaneous, however, only the last 20 ns of each simulated intermediate state was used for the calculation of $\Delta G^{\text{membrane}}_{\text{HMI}-1a3\rightarrow\text{PYR}-1gP}$ and last 11 ns for $\Delta G^{\text{membrane+protein}}_{\text{HMI}-1a3\rightarrow\text{PYR}-1gP}$ (see SI for further details).

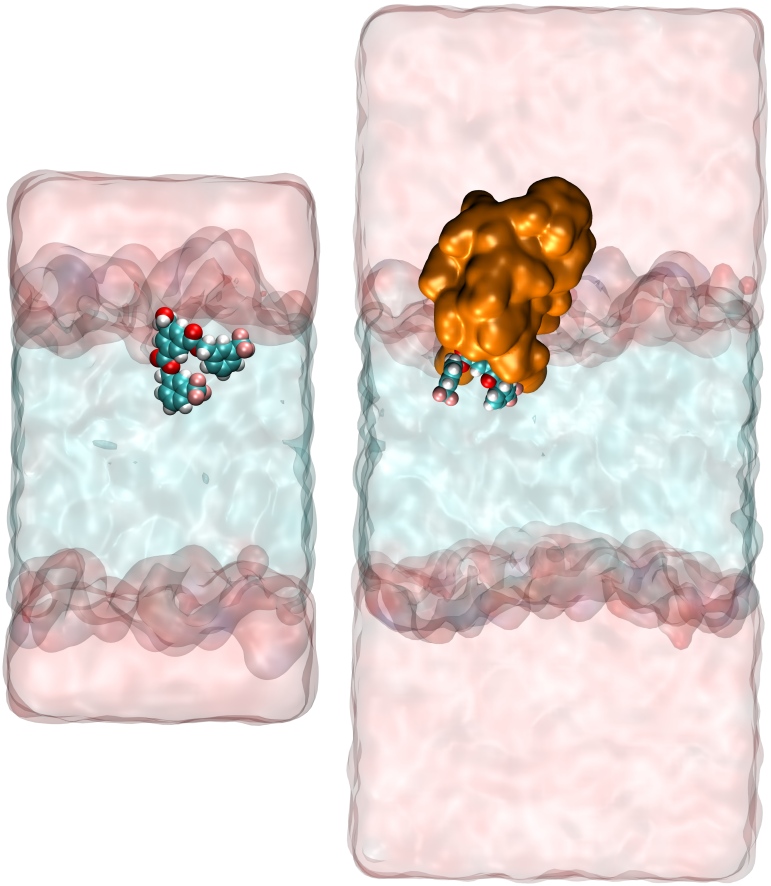

Figure 2: A schematic illustrating the starting structures for the TI calculations. The system without the PKCδ C1B domain (left) and the system with PKCδ C1B domain (right).

Simulation parameters

All simulations were run using the Gromacs simulation packages, versions 5.1.5 and 2019.4 for MD and TI, respectively[30,31,38] In all simulations the integrator used to calculate the equations of motion was the leap frog algorithm with timestep set to 2 fs. The Verlet cut-off scheme was implemented for non-bonded interactions[31] and the LINCS algorithm[39] was used on all bonds to preserve the bond length during the simulation. Temperature was set to physiological temperature (310 K) using the Nosé-Hoover thermostat[40,41] with a coupling constant of 0.4 ps in all coupling groups. Two separate thermostat coupling groups were used in the MD simulations independent of the protein; 1) lipids and ligand molecules and 2) water

and ions, while in the TI simulations, with protein present, three such groups were present: 1) protein and drug, 2) lipids and 3) water and ions. Pressure was set to atmospheric pressure (1 bar) using the Parrinello-Rahman barostat[42,43] and semi-isotropically coupled using a time constant of 10 ps in both (xy and z) directions with compressibility of 4.5×10^{-5} bar^{-1}. A cut-off radius of 1.0 nm was used for the Lennard-Jones interactions and the particle mesh Ewald method (PME)[44] with a short-range component cut-off of 1.0 nm, interpolation order of 6 and grid spacing of 0.1 nm was used for the electrostatic interactions. Periodic boundary conditions were implemented in all directions. The alchemical transformation to run the TI calculation was completed through 21 individual intermediate states with individual values for the lambda vector. First the electrostatic interactions were linearly transformed from those of HMI-1a3 to those of PYR-1gP through 10 states, followed by transformation of the Lennard-Jones interactions, bonded interactions and masses during the remaining 11 states using a soft-core potential. The soft-core alpha parameter was set to 0.5, the power of lambda in the soft-core potential set to 1 and a soft-core sigma value of 0.3 nm. The free energy change was calculated in only the immediate neighboring lambda value states.

Analysis details

All visual analysis was conducted using the VMD engine.[45] Quantitative analysis of the simulation trajectories was conducted using the aforementioned Gromacs 5.1.5 and 2019.4 simulation packages.[30,31,38] The binding free energy differences and their respective errors were found using *gmx bar* with default settings. The mass density profiles were found using *gmx density*; the results were symmetrisized with respect to the bilayer middle for clarity and smoothened with an in-house spline algorithm. The angle analysis between the ligands and the bilayer normal was calculated using *gmx gangle*, and *gmx distance* was used to determine the distance between the centers of mass of the selected groups. The orientation-distance population heat maps were obtained by combining the results of these two analyses into one plot using an in-house algorithm. H-bond analysis was conducted using *gmx hbond* with the

default donor–acceptor distance cutoff of 3.5 nm and the donor–acceptor angle cutoff of 30°. For the TI calculations, where topology did not allow the use of *gmx hbond*, the existence of the internal H-bond was judged according to the same criteria, however using the tools *gmx angle* and *gmx distance* and combining the results using an in-house algorithm.

In the simulations performed in absence of the protein, each simulation contained 4 ligand molecules. All properties, *e.g.* the number of H-bonds and SASA, were calculated for each of these four separately over the simulation trajectories using *gmx analyze* and then averaged together to report a single final result with a standard deviation as an error estimate.

NMR Spectroscopy

^{1}H NMR spectra were acquired on a Bruker Ascend 400 MHz - Avance III HD NMR spectrometer (Bruker Corporation, Billerica, MA, USA) as solutions in $CDCl_3$ and DMSO-d_6 containing tetramethylsilane (TMS) as the internal standard. Chemical shifts (δ) are reported as parts per million (ppm) relative to the TMS peaks at 0 ppm. Deuterated solvents were acquired from Sigma-Aldrich (Schnelldorf, Germany). All spectra were processed for recorded FID files with MestReNova 14.1 software (Mestrelab Research, Santiago de Compostela, Spain).

Results and Discussion

We first conducted a visual analysis of the unbiased MD simulations with only ligands and membrane present. A striking difference in the respective behaviors of the two ligands was observed. Once equilibrated inside the membrane, the −OH group of HMI-1a3 predominantly oriented towards the lipid–water interface, while, for the case of PYR-1gP, it mostly oriented towards the hydrophobic lipid tails, *i.e.* into the membrane core. To obtain a quantitative measure of this phenomenon, we performed 1) mass density profiles along the membrane normal of both −OH group and entire molecule for both compounds (Figure 3,

for full system profiles see SI) and 2) heat maps of the populations of the orientation-position relations of the −OH groups (Figure 4). The orientation of the ligand is described by the angle θ between the membrane normal and the ligand axis vector (see Figure 4, inserts).

The mass density profiles indicated that, for the case of HMI-1a3, the −OH group is positioned closer to the phosphate headgroups of the membrane lipids than the rest of the molecule, while, for the case of PYR-1gP, this does not occur (Figure 3). The orientation-distance population heat maps also demonstrated a significant difference in behavior between the two ligands: for HMI-1a3, the −OH group resides predominantly just underneath the position of the lipid phosphate headgroups with $\theta \lesssim 40°$ while, for PYR-1gP, the −OH group resides deeper within the membrane with $\theta \gtrsim 100°$ (Figure 4).

The different orientations of the two molecules directly affect the degree of exposure of their −OH group at the membrane surface. We quantified this exposure by calculating the solvent accessible surface area (SASA) of the −OH groups of the two ligands throughout the trajectories of the unbiased MD simulations, with only the ligands and membrane present. The measurement revealed a two-fold larger SASA value for HMI-1a3 in comparison to the case for PYR-1gP (0.08 ± 0.02 nm^2 and 0.04 ± 0.03 nm^2, respectively). We also calculated the SASA of the ester group oxygens (Figure 1, green) for both compounds and found the difference between the values of this property for each to be negligible (0.07 ± 0.015 nm^2 and 0.08 ± 0.04 nm^2 for HMI-1a3 and PYR-1gP, respectively).

The TI calculation, with the PKCδ C1B domain present, revealed a $\Delta\Delta G^{\text{protein}}_{\text{HMI}-1a3\rightarrow\text{PYR}-1gP}$ of ∼29 kJ/mol (see Table S2 for separate values). This indicates a substantial difference in binding affinities between the compounds and suggests the existence of a prominent competing interaction is the cause of the diminished binding affinity. Visual inspection and H-bonding analysis over the TI intermediate state simulation trajectories revealed the mechanism for this: as the electrostatic and van der Waals forces change from those of HMI-1a3 to PYR-1gP, an internal H-bond between the −OH (H-donor) and a nitrogen (H-acceptor) of the central heterocycle forms (see Figure S2). We further observed that, as this intramolec-

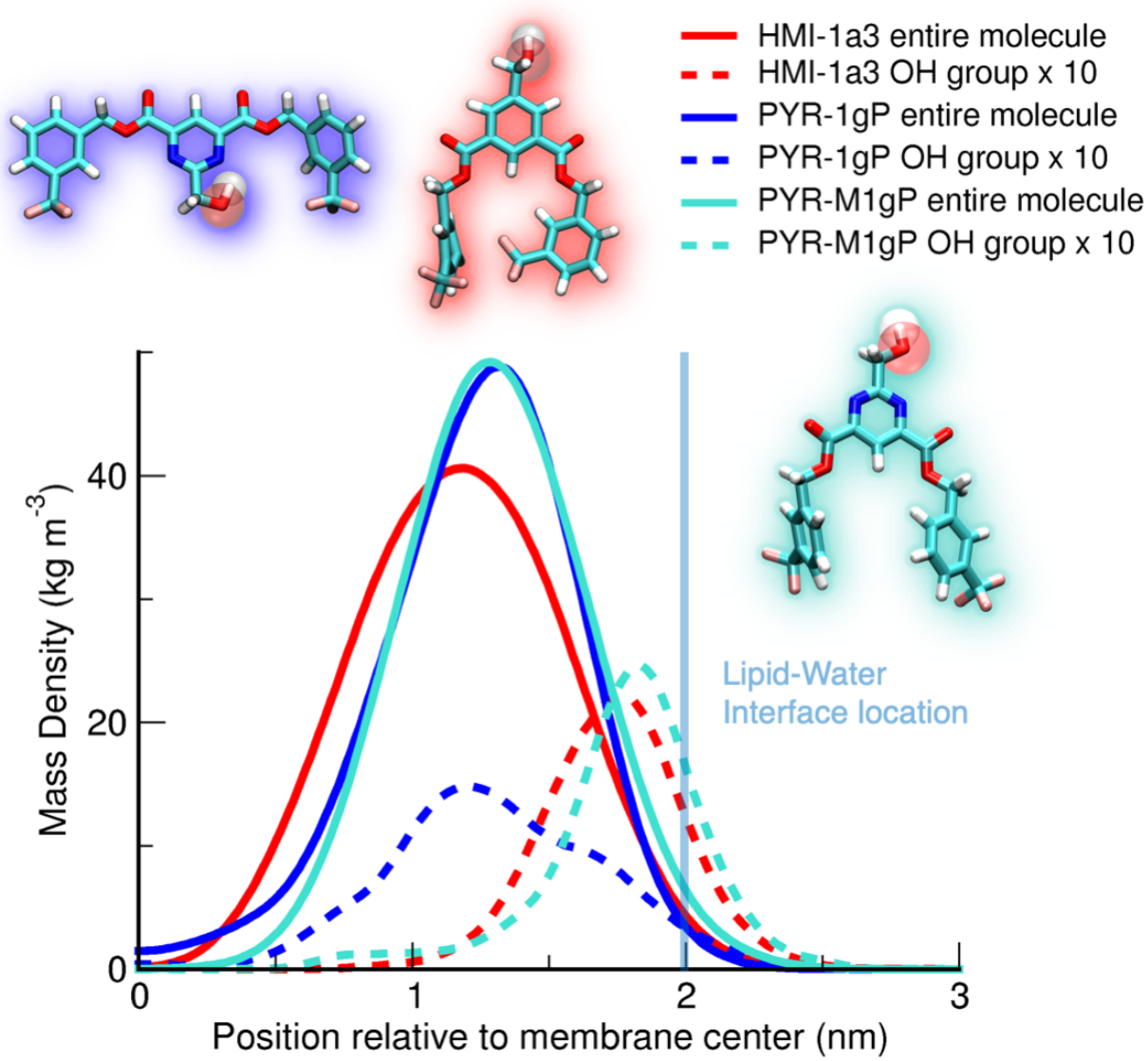

Figure 3: Mass density profiles of PYR-1gP, HMI-1a3 (unbiased MD), and the biased pyrimidine PYR-M1gP (steered MD), each highlighted with blue, red and cyan, respectively.

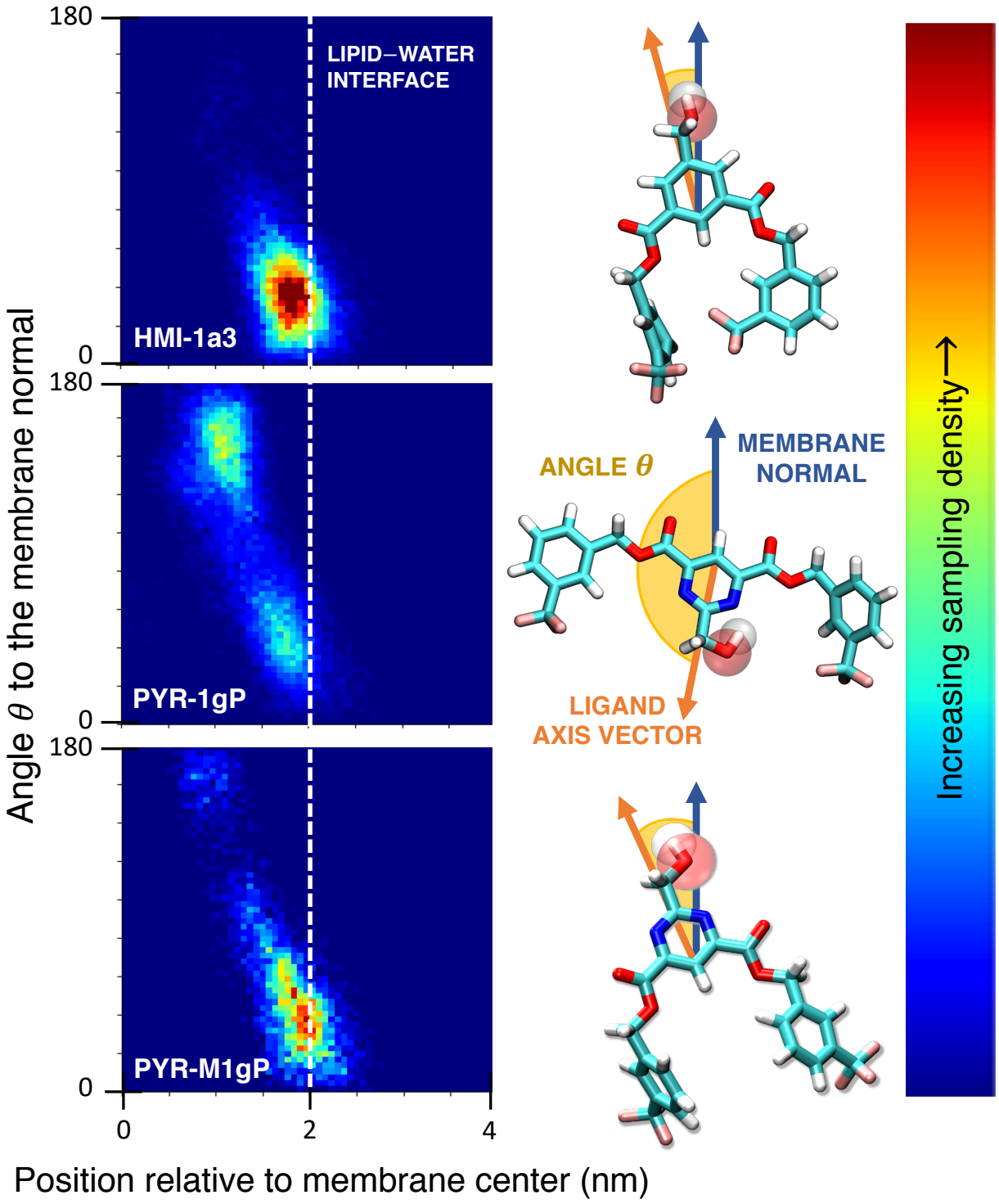

Figure 4: Heatmaps that demonstrate the populations of orientation-position relations of the −OH groups during the simulations, along with illustrations of the ligand axis vector that defines the angle θ.

ular H-bond arises, it disrupts the interactions of the −OH group with Leu251 (backbone C=O) and Thr242 (backbone NH) of the PKCδ C1B domain that have previously been found to be crucial for binding.[7–9] Interestingly, our calculations revealed that the additional interaction between the −OH group and Thr242 (backbone C=O), also suggested by previous docking studies,[8,9] did not occur during the entire duration of the TI calculation. Another predicted interaction between the ligand and residue Gly253, instead, remained relatively undisturbed (see Figure S2).

Upon observing this phenomenon in the TI simulations with the protein present, we investigated the possibility of similar behavior in the unbiased MD simulations, performed in absence of the protein. We calculated the frequency of the occurrence of intramolecular H-bonds per ligand over the simulation time and that of H-bonds between the ligand −OH group and water. The internal H-bonding in PYR-1gP appeared throughout these simulations with an average of 0.46 ± 0.01 internal H-bonds per ligand over the entire simulation time, *i.e.* 46% of the time the H-bond between N and −OH was present. For HMI-1a3 no such internal H-bonding occurred. As expected, in PYR-1gP the amount of H-bonding between ligand −OH group and water was greatly decreased in comparison to the case for HMI-1a3 (0.28 ± 0.3 and 0.97 ± 0.11 H-bonds per ligand, respectively). The extent of intramolecular H-bonding in PYR-1gP together with the decrease in H-bonding with water in these simulations can be seen to directly correlate with the observed breakage of the −OH group H-bonds with Leu251 and Thr242 in the TI simulations with protein, as the formation of the intramolecular bond disrupts other bonding.

The key difference between the two compounds was thus the ability, or lack thereof, to form the intramolecular H-bond. The effect of H-bonds has been previously observed to be significant; Ryckbosch *et al.* reported that H-bonding of the ligand in the membrane environment can greatly affect the behavior of PKC.[46] They demonstrated that H-bonding between the PKCδ C1B domain–bound ligand and water molecules at the lipid–water interface, *i.e.* the hydrated region of the membrane, could control the orientation and depth of insertion of

the whole protein–ligand complex, possibly explaining the reason different ligands can cause different modes of action of the same enzyme.[46]

Our results indicated that, also in this case, H-bonding affects the orientations of the ligand–protein complex components. When considering the SASA values and the extent of H-bonding of the ligands in our simulations, a virtual axis across the ester oxygens, perpendicular to the membrane normal, can be seen to acts as a hinge through which the molecule rotates when the internal H-bond forms between the −OH group and N atom of the pyrimidine core while the ligand is within the lipid membrane.

To determine whether or not the internal H-bond is the cause of this flip in membrane orientation, we conducted a steered MD simulation in which a bias potential prevented the observed H-bond formation in PYR-1gP; we identified the resulting structure as PYR-M1gP. Analysis of the trajectory of the simulation of this new structure in the membrane without the protein revealed that when the H-bond was effectively removed through the biasing potential, the resulting behavior of PYR-M1gP was almost identical to that of HMI-1a3 in both the mass density profile (Figure 3) and the distance-orientation population heat map (Figure 4). As expected, a notably increased extent of H-bonding with water was also observed in comparison to the case for unbiased PYR-1gP; on average 0.66 ± 0.09 H-bonds per ligand was observed over the entire simulation time. The similarity of the behavior of PYR-M1gP to that of HMI-1a3 indicates that, as suspected, the intramolecular H-bond that we see to form in PYR-1gP does indeed bring about the observed flip in the molecular orientation.

To provide complementary experimental insight into the internal H-bond in PYR-1gP seen in our MD simulations, we turned to NMR spectroscopy. We chose the readily available symmetrical pyrimidine PYR-1b (Figure 5) to verify the solvent accessibility of the −OH group and compared the ^{1}H NMR spectra of the compound measured in $CDCl_3$ and DMSO-d_6, respectively. According to Jansma *et al.*[47] and Jennings *et al.*,[48] solvent-accessible hydrogen atoms typically show a difference of chemical shifts (Δppm) of Δppm $CDCl_3 \rightarrow$

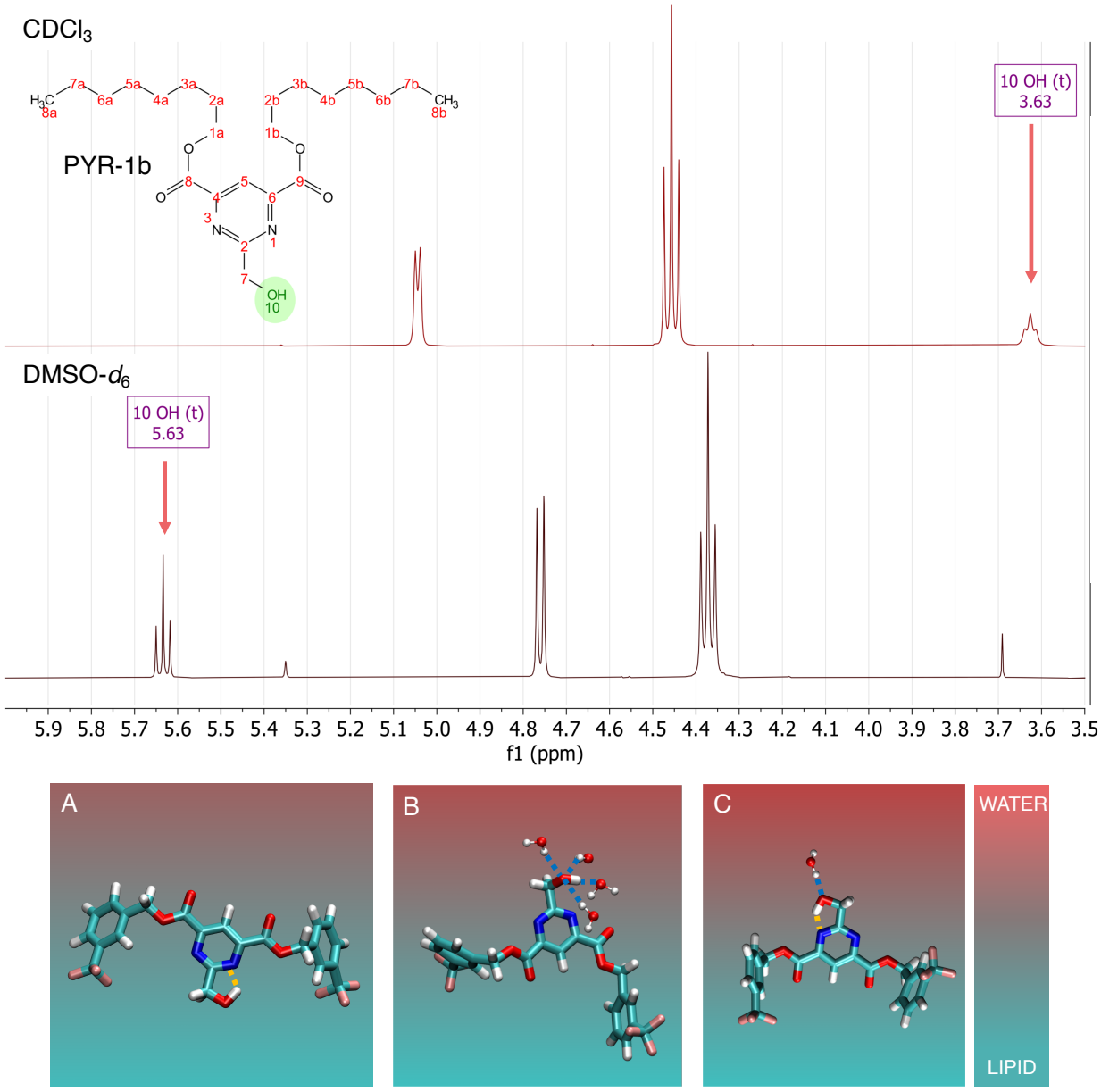

Figure 5: NMR-study of the intramolecular hydrogen bond in PYR-1b with simulation snapshots of PYR-1gP. A) Hydrogen bond in the membrane core *i.e.* in the absence of polar solvent. B) and C) The possible hydrogen bonding at the membrane–water interface, *i.e.* in the presence of polar solvent. In B we see disruption of the internal hydrogen bond by the water solvent and in C a case where this does not occur.

DMSO-d_6 = 2–4 ppm, while those engaged in a strong H-bond show Δppm $CDCl_3 \rightarrow$ DMSO-d_6 < 1 ppm. In our case, the signal relative to the −OH group of interest shows a Δppm $CDCl_3 \rightarrow$ DMSO-d_6 = 2 ppm (Figure 5). This would suggest that no strong intramolecular hydrogen bond forms in the environment of the NMR experiment.

As previously mentioned, the MD simulations carried out in absence of the protein, indicate that the extent of internal H-bonding per PYR-1gP ligand is 0.46±0.01, a substantial extent, though not present at all times. Visual analysis of the H-bonding in these simulations revealed that, in specific cases, when multiple water molecules coordinate correctly around the −OH group at the lipid–water interface, the aforementioned internal H-bond can indeed be disrupted (Figure 5B), however there also exist cases where the water solvent is not able to perturb it (Figure 5C). This is especially the case when the ligand is embedded deeper within the apolar lipid tails, thus leaving the H-bond inaccessible to the solvent (Figure 5A). While the NMR experiment did not reveal the presence of a strong H-bond in polar solvent environment, this does not exclude the possibility of such an H-bond interaction emerging in the apolar environment of the lipid core of the membrane.

To assess the manner in which the polarity of the environment affects intramolecular H-bonding, we determined, through QM calculation, the strength of the dihedral interaction controlling the H-bond *i.e.* the conformational energy as a function of the dihedral interaction angle to the −OH group in the compounds: C−C−C−O for HMI-1a3 and N−C−C−O for PYR-1gP (see Figure S7), in both polar and apolar environments (Figure 6). This revealed that the C−C−C−O dihedral interaction in HMI-1a3 is relatively unaffected by the extent of the polarity of its environment, while the N−C−C−O dihedral interaction in PYR-1gP is very sensitive to the polarity of its surroundings.

In PYR-1gP the strength of the N−C−C−O dihedral interaction, *i.e.* intramolecular H-bond, is greatly amplified in the vacuum environment used to model the hydrophobic and apolar membrane core; the depth of the minimum, thus probability of H-bond formation, doubles when PYR-1gP is in vacuum instead of polar solvent conditions. This observation

suggests that the internal H-bond in PYR-1gP is much easier to disrupt in polar solvent, *e.g.* the measurement conditions for the NMR experiment. Once within the membrane core, the same bond is significantly strengthened, thus unlikely to break. This could explain the lack of binding of PYR-1gP to the C1 domain of PKC, even though our NMR results did not conclusively indicate the existence of the said bond.

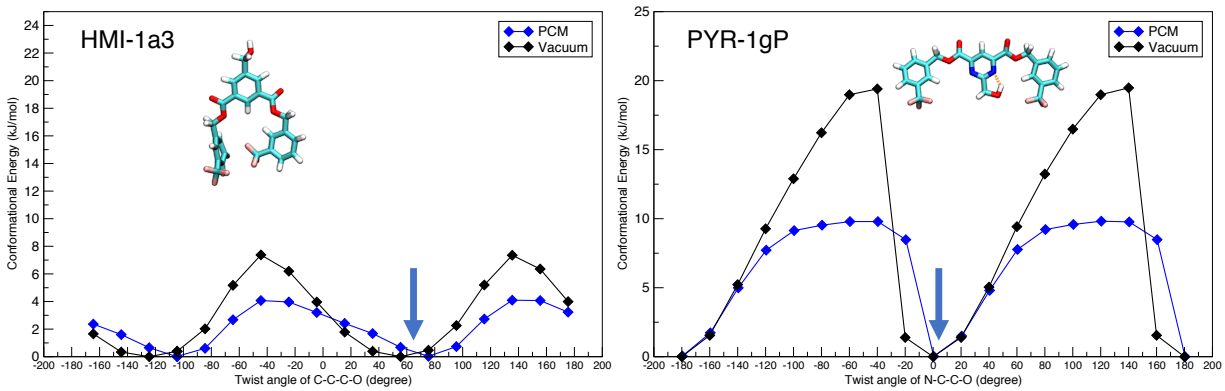

Figure 6: Calculation of the conformational energy as a function of angle for the dihedral interaction to the −OH group for both compounds. Note the different positions of the energy minima (blue arrows), indicating lack of intramolecular H-bond in HMI-1a3 (left) and the presence of an intramolecular H-bond in compound PYR-1gP (right).

These QM calculations also offer further support for the existence of the internal H-bond. Notably for PYR-1gP the angle of minimum conformational energy was 0° instead of ∼75°, the case for HMI-1a3 (see Figure 6), and the depths of the minima were significantly greater than those for HMI-1a3 in both polar and apolar environments. This result explicitly demonstrates the presence of the H-bond, between the N and H atoms in PYR-1gP, already observed in the MD simulations discussed earlier. Collectively the QM and NMR results suggest that only in the lipid environment is the intramolecular H-bond sufficiently pronounced so as to cause the effects detected by the simulations.

Even though our simulations only dealt with HMI-1a3 and PYR-1gP specifically, it is reasonable to expect similar behavior from homologous ligands within the respective series.[8,9] As their central scaffold is constant, *i.e.* aromatic core, two hydrophobic substituents and hydroxymethyl group, it is safe to assume minimal changes in their respective behavior in

the membrane environment in comparison to that of PYR-1gP, given that the other two substituents maintain comparable hydrophobic properties; this insight may thus assist in the development of the next generation of PKC modulators. The current work models the conditions in the aforementioned binding assay;[8,9] the same computational methodology can, however, be used in future studies using lipid membranes that more closely match the appropriate biomembranes.

Moreover, the issues raised by our study of PKC activators are more widely applicable to the broader context of weakly membrane-associated proteins (bitopic and peripheral). Unlike the case for integral membrane proteins, for weakly membrane-associated proteins the number of drug design studies that take into consideration the role of the lipid membrane is quite limited. At the same time, a large number of publications have found evidence of a strong affinity of numerous drugs for lipid bilayers[49,50] and others have demonstrated that the membrane plays a significant role in substrate selection, in spite of the fact that catalysis occurs outside the membrane core.[51] In a previous work, for example, we investigated the role the lipid membrane plays in substrate selection in a different weakly membrane-associated protein, the membrane bound isoform of catechol-*O*-methyltransferase (MB-COMT).[52] It is worth noting that, in addition to affecting the direct ligand–protein interactions explored here, the membrane can also cause other substantial effects too. The lipophilicity of a ligand is believed to affect its kinetics due to the reduction of dimensionality of diffusion from three to two dimensions (membrane plane);[53] additionally, the accumulation of drug molecules in the membrane increases local drug concentration, which, in turn, leads to an increase in the rate of drug–target protein association.[54] Altogether, for any protein that is in any way membrane-associated, even weakly, the membrane will most likely play an important role in both ligand and substrate selection, thus the inclusion of its role proves essential in drug design.

Conclusions

In this work, we aimed to determine the cause of the greatly diminished binding of the pyrimidine analogs of the isophthalate derivatives to the C1 domain of PKC. We achieved this through examination of two specific compounds, HMI-1a3 and PYR-1gP, in a multi-faceted study utilizing comprehensive molecular modeling, electronic structure calculations and NMR measurements.

Altogether, our results suggest that ignoring the presence of the lipid membrane in the *in silico* assessment of ligand binding, *i.e.* docking, can cause false predictions of binding affinity. Here, for the case of scaffold hopping from isophthalate to pyrimidine derivatives, it was in fact the lipid membrane environment that caused the discrepancies in affinity towards PKC between the two ligands. While usually replacing a phenyl ring with a pyrimidine increases ligand solubility and thus also bioavailability, in this specific case, the intrinsic propensity for H-bonding of the H and N atoms in PYR-1gP was amplified by the apolar membrane environment; the apolar lipid membrane conditions push PYR-1gP to form a strong enough intramolecular H-bond to reduce the affinity for PKC by leading the ligand to invert its orientation, directing the −OH group towards the membrane core. This, in turn, decreases the exposure of the key functional group at the lipid–water interface where binding takes place and leaves PYR-1gP very unlikely to interact with the PKC C1 domain. Simultaneously, even though the other favorable orientation exposing the −OH group also exists for PYR-1gP, the TI calculations showed that the internal hydrogen bond also directly occupies the −OH group, preventing binding to the C1 domain. Binding is thus unlikely in either orientation, explaining the lack of binding witnessed in our previous study.[9]

In summary, through molecular modeling, we reveal the unexpected reason for the diminished binding affinity of the 2-methylhydroxy pyrimidines, designed as more hydrophilic PKC modulators by scaffold hopping from their predecessor (5-hydroxymethyl)isophthalates. The culprit, largely due to the membrane environment, is the internal H-bond between the −OH group (H-donor) and a nitrogen (H-acceptor) of the pyrimidine core. Our study also

reinforces the shortcomings of standard docking calculations for some weakly membrane-associated proteins where the lipid membrane plays a role in ligand selection and highlights the need for a more rigorous computational approach, that explicitly takes the role of the associated membrane into account, as we have carried out in this study.

Acknowledgement

The authors thank the Orion Foundation (S.L), the University of Helsinki Doctoral Programme of Drug Research (S.L.), the University of Helsinki Drug Research Program (S.L & R.P.), the Finnish Cultural Foundation (R.P.), the Academy of Finland Grant 298863 (postdoctoral grant, A.K.), the Sigrid Juselius Foundation (V.T.), the Finnish Foundation for Cardiovascular Research (V.T), the Academy of Finland Grant 321564 (V.T.) and the Academy of Finland Grant 287963 (A.B) for financing this research. All simulations were carried out using the resources provided by CSC IT Center for Science Ltd. We thank Ilari Tarvainen, Giray Enkavi, Evgeni Grazhdankin and Gustav Boije af Gennäs for advice and discussions. We also thank Prof. Stuart Conway for the fruitful discussion about the NMR methods used in this study.

PDB ID codes

1PTR, PKC δ C1B domain

Supporting Information Available

The following files are available free of charge. Authors will release the atomic coordinates and experimental data upon article publication.

- Supporting Information: Details of the system compositions, equilibration of the trajectories, protein topology preparation, parameterisation of dihedral potentials for

HMI-1a3, PYR-1gP and PYR-M1gP, discussion on the chosen ligand parameterisation scheme, full partial mass density profiles for simulations in absence of protein and graphical representation of H-bond analysis in TI simulations (PDF)

- Atomic coordinates and required topology files for molecules used in simulations (.gro and .itp)
- Molecular formula strings (CSV)
- Videos of the restrains holding the Zn^{+2} coordinated secondary structure: SV1; equilibration run and SV2; an example of a TI run (State 10).

References

(1) Newton, A. C.; Brognard, J. Reversing the Paradigm: Protein Kinase C as a Tumor Suppressor. *Trends Pharmacol. Sci.* **2017**, *38*, 438–447.

(2) Newton, A. C. Protein kinase C: perfectly balanced. *Crit. Rev. Biochem. Mol. Biol.* **2018**, *53*, 208–230.

(3) Talman, V.; Pascale, A.; Jäntti, M.; Amadio, M.; Tuominen, R. K. Protein Kinase C Activation as a Potential Therapeutic Strategy in Alzheimer's Disease: Is there a Role for Embryonic Lethal Abnormal Vision-like Proteins? *Basic Clin. Pharmacol. Toxicol.* **2016**, *119*, 149–160.

(4) Antal, C. E.; Hudson, A. M.; Kang, E.; Zanca, C.; Wirth, C.; Stephenson, N. L.; Trotter, E. W.; Gallegos, L. L.; Miller, C. J.; Furnari, F. B.; Hunter, T.; Brognard, J.; Newton, A. C. Cancer-Associated Protein Kinase C Mutations Reveal Kinase's Role as Tumor Suppressor. *Cell* **2015**, *160*, 489–502.

(5) Rahman, G. M.; Das, J. Modeling studies on the structural determinants for the

DAG/phorbol ester binding to C1 domain. *J. Biomol. Struct. Dyn.* **2015**, *33*, 219–232.

(6) Das, J.; Rahman, G. M. C1 Domains: Structure and Ligand-Binding Properties. *Chem. Rev.* **2014**, *114*, 12108–12131.

(7) Li, J.; Ziemba, B. P.; Falke, J. J.; Voth, G. A. Interactions of protein kinase C-α C1A and C1B domains with membranes: a combined computational and experimental study. *J. Am. Chem. Soc.* **2014**, *136*, 11757–11766.

(8) Boije af Gennäs, G.; Talman, V.; Aitio, O.; Ekokoski, E.; Finel, M.; Tuominen, R. K.; Yli-Kauhaluoma, J. Design, Synthesis, and Biological Activity of Isophthalic Acid Derivatives Targeted to the C1 Domain of Protein Kinase C. *J. Med. Chem.* **2009**, *52*, 3969–3981, PMID: 19438240.

(9) Provenzani, R.; Tarvainen, I.; Brandoli, G.; Lempinen, A.; Artes, S.; Turku, A.; Jäntti, M. H.; Talman, V.; Yli-Kauhaluoma, J.; Tuominen, R. K.; Boije af Gennäs, G. Scaffold hopping from (5-hydroxymethyl) isophthalates to multisubstituted pyrimidines diminishes binding affinity to the C1 domain of protein kinase C. *PLoS One* **2018**, *13*, 1–27.

(10) Talman, V.; Tuominen, R. K.; Boije af Gennäs, G.; Yli-Kauhaluoma, J.; Ekokoski, E. C1 Domain-targeted isophthalate derivatives induce cell elongation and cell cycle arrest in HeLa cells. *PloS One* **2011**, *6*, e20053; e20053–e20053.

(11) Jäntti, M. H.; Talman, V.; Räsänen, K.; Tarvainen, I.; Koistinen, H.; Tuominen, R. K. Anticancer activity of the protein kinase C modulator HMI-1a3 in 2D and 3D cell culture models of androgen-responsive and androgen-unresponsive prostate cancer. *FEBS Open Bio* **2018**, *8*, 817–828.

(12) Pantsar, T.; Poso, A. Binding Affinity via Docking: Fact and Fiction. *Molecules* **2018**, *23*, 1899.

(13) Pasenkiewicz-Gierula, M.; Baczynski, K.; Markiewicz, M.; Murzyn, K. Computer modelling studies of the bilayer/water interface. *Biochim. Biophys. Acta, Biomembr.* **2016**, *1858*, 2305–2321.

(14) Frisch, M. J. et al. Gaussian 16 Revision B.01. 2016; Gaussian Inc. Wallingford CT.

(15) Becke, A. D. Density-functional thermochemistry. III. The role of exact exchange. *J. Chem. Phys.* **1993**, *98*, 5648–5652.

(16) Stephens, P. J.; Devlin, F. J.; Chabalowski, C. F.; Frisch, M. J. Ab Initio Calculation of Vibrational Absorption and Circular Dichroism Spectra Using Density Functional Force Fields. *J. Phys. Chem.* **1994**, *98*, 11623–11627.

(17) Ditchfield, R.; Hehre, W. J.; Pople, J. A. Self-Consistent Molecular-Orbital Methods. IX. An Extended Gaussian-Type Basis for Molecular-Orbital Studies of Organic Molecules. *J. Chem. Phys.* **1971**, *54*, 724–728.

(18) Miertuš, S.; Scrocco, E.; Tomasi, J. Electrostatic interaction of a solute with a continuum. A direct utilizaion of AB initio molecular potentials for the prevision of solvent effects. *Chem. Phys.* **1981**, *55*, 117–129.

(19) Miertuš, S.; Tomasi, J. Approximate evaluations of the electrostatic free energy and internal energy changes in solution processes. *Chem. Phys.* **1982**, *65*, 239–245.

(20) Pascual-ahuir, J. L.; Silla, E.; Tuñon, I. GEPOL: An improved description of molecular surfaces. III. A new algorithm for the computation of a solvent-excluding surface. *J. Comput. Chem.* **1994**, *15*, 1127–1138.

(21) Dunning, T. H. Gaussian basis sets for use in correlated molecular calculations. I. The atoms boron through neon and hydrogen. *J. Chem. Phys.* **1989**, *90*, 1007–1023.

(22) Singh, U. C.; Kollman, P. A. An approach to computing electrostatic charges for molecules. *J. Comput. Chem.* **1984**, *5*, 129–145.

(23) Bayly, C. I.; Cieplak, P.; Cornell, W.; Kollman, P. A. A well-behaved electrostatic potential based method using charge restraints for deriving atomic charges: the RESP model. *J. Phys. Chem.* **1993**, *97*, 10269–10280.

(24) Case, D. et al. AMBER18. University of California: San Fransisco, 2018.

(25) Wang, J.; Wang, W.; Kollman, P. A.; Case, D. A. Automatic atom type and bond type perception in molecular mechanical calculations. *J. Mol. Graphics Modell.* **2006**, *25*, 247–260.

(26) Jo, S.; Kim, T.; Iyer, V. G.; Im, W. CHARMM-GUI: A web-based graphical user interface for CHARMM. *J. Comput. Chem.* **2008**, *29*, 1859–1865.

(27) Wu, E. L.; Cheng, X.; Jo, S.; Rui, H.; Song, K. C.; Dávila-Contreras, E. M.; Qi, Y.; Lee, J.; Monje-Galvan, V.; Venable, R. M.; Klauda, J. B.; Im, W. CHARMM-GUI Membrane Builder toward realistic biological membrane simulations. *J. Comput. Chem.* **2014**, *35*, 1997–2004.

(28) Zhang, G.; Kazanietz, M. G.; Blumberg, P. M.; Hurley, J. H. Crystal structure of the Cys2 activator-binding domain of protein kinase Cδ in complex with phorbol ester. *Cell* **1995**, *81*, 917–924.

(29) Jorgensen, W. L.; Maxwell, D. S.; Tirado-Rives, J. Development and Testing of the OPLS All-Atom Force Field on Conformational Energetics and Properties of Organic Liquids. *J. Am. Chem. Soc.* **1996**, *118*, 11225–11236.

(30) Abraham, M. J.; Murtola, T.; Schulz, R.; Páll, S.; Smith, J. C.; Hess, B.; Lindahl, E. GROMACS: High performance molecular simulations through multi-level parallelism from laptops to supercomputers. *SoftwareX* **2015**, *1-2*, 19–25.

(31) Abraham, M.; van der Spoel, D.; Lindahl, E.; Hess, B.; the GROMACS development team, GROMACS User Manual version 5.1.5. 2017.

(32) Ribeiro, A. S. T.; Horta, B. A. C.; Alencastro, R. B. d. MKTOP: a program for automatic construction of molecular topologies. *J. Braz. Chem. Soc.* **2008**, *19*, 1433–1435.

(33) Maciejewski, A.; Pasenkiewicz-Gierula, M.; Cramariuc, O.; Vattulainen, I.; Rog, T. Refined OPLS All-Atom Force Field for Saturated Phosphatidylcholine Bilayers at Full Hydration. *J. Phys. Chem. B* **2014**, *118*, 4571–4581.

(34) Kulig, W.; Pasenkiewicz-Gierula, M.; Róg, T. Cis and trans unsaturated phosphatidylcholine bilayers: A molecular dynamics simulation study. *Chem. Phys. Lipids* **2016**, *195*, 12–20.

(35) Jorgensen, W. L.; Chandrasekhar, J.; Madura, J. D.; Impey, R. W.; Klein, M. L. Comparison of simple potential functions for simulating liquid water. *J. Chem. Phys.* **1983**, *79*, 926–935.

(36) Dang, L. X.; Schenter, G. K.; Glezakou, V.-A.; Fulton, J. L. Molecular Simulation Analysis and X-ray Absorption Measurement of Ca2+, K+ and Cl- Ions in Solution. *J. Phys. Chem. B* **2006**, *110*, 23644–23654.

(37) Michel, J.; Essex, J. W. Prediction of protein–ligand binding affinity by free energy simulations: assumptions, pitfalls and expectations. *J. Comput.-Aided Mol. Des.* **2010**, *24*, 639–658.

(38) Abraham, M.; van der Spoel, D.; Lindahl, E.; Hess, B.; the GROMACS development team, GROMACS User Manual version 2019.4. 2019.

(39) Hess, B.; Bekker, H.; Berendsen, H. J. C.; Fraaije, J. G. E. M. LINCS: A linear constraint solver for molecular simulations. *J. Comput. Chem.* **1997**, *18*, 1463–1472.

(40) Nosé, S. A molecular dynamics method for simulations in the canonical ensemble. *Mol. Phys.* **1984**, *52*, 255–268.

(41) Hoover, W. G. Canonical dynamics: Equilibrium phase-space distributions. *Phys. Rev. A* **1985**, *31*, 1695–1697.

(42) Parrinello, M.; Rahman, A. Polymorphic transitions in single crystals: A new molecular dynamics method. *J. Appl. Phys. (Melville, NY, U. S.)* **1981**, *52*, 7182–7190.

(43) Nosé, S.; Klein, M. L. Constant pressure molecular dynamics for molecular systems. *Mol. Phys.* **1983**, *50*, 1055–1076.

(44) Essmann, U.; Perera, L.; Berkowitz, M. L.; Darden, T.; Lee, H.; Pedersen, L. G. A smooth particle mesh Ewald method. *J. Chem. Phys.* **1995**, *103*, 8577–8593.

(45) Humphrey, W.; Dalke, A.; Schulten, K. VMD: Visual molecular dynamics. *J. Mol. Graphics* **1996**, *14*, 33–38.

(46) Ryckbosch, S. M.; Wender, P. A.; Pande, V. S. Molecular dynamics simulations reveal ligand-controlled positioning of a peripheral protein complex in membranes. *Nat. Commun.* **2017**, *8*, 6.

(47) Jansma, A.; Zhang, Q.; Li, B.; Ding, Q.; Uno, T.; Bursulaya, B.; Liu, Y.; Furet, P.; Gray, N. S.; Geierstanger, B. H. Verification of a Designed Intramolecular Hydrogen Bond in a Drug Scaffold by Nuclear Magnetic Resonance Spectroscopy. *J. Med. Chem.* **2007**, *50*, 5875–5877.

(48) Jennings, L. E. et al. BET bromodomain ligands: Probing the WPF shelf to improve BRD4 bromodomain affinity and metabolic stability. *Bioorg. Med. Chem.* **2018**, *26*, 2937–2957.

(49) Kopeć, W.; Telenius, J.; Khandelia, H. Molecular dynamics simulations of the interactions of medicinal plant extracts and drugs with lipid bilayer membranes. *FEBS J.* **2013**, *280*, 2785–2805.

(50) Cramariuc, O.; Róg, T.; Vattulainen, I. Drug-Lipid Membrane Interaction Mechanisms Revealed Through Molecular Simulations. *Curr. Phys. Chem.* **2012**, *2*, 379–400.

(51) Robinson, R. G. et al. Characterization of Non-Nitrocatechol Pan and Isoform Specific Catechol-O-methyltransferase Inhibitors and Substrates. *ACS Chem. Neurosci.* **2012**, *3*, 129–140.

(52) Magarkar, A.; Parkkila, P.; Viitala, T.; Lajunen, T.; Mobarak, E.; Licari, G.; cramariuc, O.; Vauthey, E.; Róg, T.; Bunker, A. Membrane bound COMT isoform is an interfacial enzyme: General mechanism and new drug design paradigm. *Chem. Commun. (Cambridge, U. K.)* **2018**, *54*, 3440 – 3443.

(53) Vauquelin, G.; Packeu, A. Ligands, their receptors and ... plasma membranes. *Mol. Cell. Endocrinol.* **2009**, *311*, 1–10.

(54) Sykes, D. A.; Parry, C.; Reilly, J.; Wright, P.; Fairhurst, R. A.; Charlton, S. J. Observed Drug-Receptor Association Rates Are Governed by Membrane Affinity: The Importance of Establishing "Micro-Pharmacokinetic/Pharmacodynamic Relationships" at the β-Adrenoceptor. *Mol. Pharmacol.* **2014**, *85*, 608.

Graphical TOC Entry